Supplementary Material

Tuning magnetic anisotropy by the p-bonding features of the axial ligands and the electronic effects of gold(I) atoms in CoN_4X_2 (X =N, O) field induced Single-Ion Magnets nodes of 2D $\{Co(L)_2[Au(CN)_2]_2\}_n$ metal-organic frameworks.

María A. Palacios, Ismael F. Díaz-Ortega, Hiroyuki Nojiri, Elizaveta A. Suturina, Mykhaylo Ozerov, J. Krzystek, Enrique Colacio

Table S1.- Crystallographic data for complexes **1**, **3**-**5**.

Compound	**1(DMSO)**	**3 (py)**	**4(bzpy)**	**5 (naphthalene)**
Formula	$C_8H_{12}Au_2CoN_4O_2S_2$	$C_7H_5AuCo_{0.5}N_3$	$C_{28}H_{18}Au_2CoN_6O_2$	$C_{34}H_{26}Au_2CoN_6$
M_r	713.20	357.57	923.35	971.47
Crystal system	Monoclinic	Monoclinic	Monoclinic	Monoclinic
Space group	$P2_1/c$	$P2_1/c$	$P2_1/c$	C2/c
a (Å)	7.4006(3)	7.1352(3)	13.1531(5)	20.2748(17)
b (Å)	14.3681(5)	13.9841(6)	13.5483(5)	10.4871(7)
c (Å)	14.9002(6)	8.4042(4)	15.5142(5)	16.0466(12)
a (°)	90	90	90	90
β (°)	93.6693(18)	95.735(2)	93.7020(17)	115.017(2)
γ (°)	90	90	90	90
V (Å^3)	1581.13(11)	834.37(6)	2758.90(17)	3091.8(4)
Z	4	4	4	4
Dc (g cm^{-1})	2.996	2.847	2.223	2.087
m(MoK_a) (mm^{-1})	19.813	18.528	11.240	10.031
T (K)	100(2)	293(2)	100(2)	100(2)
Observed reflections [a]	4075 (3335)	2135 (2103)	6398 (4724)	3190 (3120)
R_{int}	0.0362	0.0333	0.0585	0.0611
Parameters	176	106	352	199
GOF	1.320	0.747	0.814	0.700
R_1 [b,a]	0.0485 (0.0372)	0.0182 (0.0179)	0.0562 (0.0317)	0.0290 (0.0276)

wR_2 [c,a]	0.1747 (0.1669)	0.0768 (0.0701)	0.1176 (0.0945)	0.0750 (0.0737)

[a] Values in parentheses for reflections with $I > 2\sigma(I)$.

[b] $R_1 = ||Fo| - |Fc||/\Sigma|Fo|$.

[c] $wR_2 = \{\Sigma[w(Fo^2 - Fc^2)^2] / \Sigma[w(Fo^2)^2]\}^{½}$.

Table S2.- Continuous Shape Measures calculations for **1**-**5**.

S H A P E v2.1 Continuous Shape Measures calculation
(c) 2013 Electronic Structure Group, Universitat de Barcelona
Contact: llunell@ub.edu

JPPY-6 5 C5v Johnson pentagonal pyramid J2
TPR-6 4 D3h Trigonal prism
OC-6 3 Oh Octahedron
PPY-6 2 C5v Pentagonal pyramid
HP-6 1 D6h Hexagon

JPPY-6 5 C5v Johnson pentagonal pyramid J2
TPR-6 4 D3h Trigonal prism
OC-6 3 Oh Octahedron
PPY-6 2 C5v Pentagonal pyramid
HP-6 1 D6h Hexagon

Complex **1**

Structure [ML6] JPPY-6 TPR-6 OC-6 PPY-6 HP-6 33.075, 16.317, 0.038, 29.637, 32.528.

Complex **2**

Structure [ML6] JPPY-6 TPR-6 OC-6 PPY-6 HP-6, 32.149, 15.542, 0.103, 28.650, 31.823.

Complex **3**

Structure [ML6] JPPY-6 TPR-6 OC-6 PPY-6 HP-6, 33.742, 16.677, 0.003, 30.222, 33.079.

Complex **4**

Structure [ML6] JPPY-6 TPR-6 OC-6 PPY-6 HP-6, 32.096, 15.669, 0.126, 28.596, 32.303.

Complex **5**

Structure [ML6] JPPY-6 TPR-6 OC-6 PPY-6 HP-6 , 32.547, 15.837, 0.070, 29.003, 33.231

Table S3. SOC-CASSCF(7,5)/NEVPT2 computed eigenvalues of the effective g-tensor of the lowest Kramers doublet (the values calculated including gold(I) atoms are given in red color)

Compound	g'_1	g'_2	g'_3
DMF	2.610	4.864	5.598
	2.176	2.805	7.363
DMSO	2.433	3.344	6.940
	1.924	3.324	6.900
Pyridine	1.985	3.614	6.684
	2.262	4.217	6.104
PyPhCO	1.956	4.130	6.294
	2.622	4.598	5.570

Table S4. S_{eff} = 1/2 Hamiltonian parameters determined from HFEPR of the investigated complexes.

	g_x	g_y	g_z
Co-Au-DMSO **1**	6.05	3.59	1.92
Co-Au-DMF **2**	2.65	2.95	6.55
Co-Au-Py **3**	5.21	4.60	2.58
Co-Au-BzPy **4**	3.15	3.78	5.58

Table S5. Spin Hamiltonian parameters computed with SOC-CASSCF(7,5)/NEVPT2 for **1-4** and obtained by different experimental techniques.

	Method	D, cm^{-1}	E/D	$\delta = 2\sqrt{D^2 + 3E^2}$	g_1	g_2	g_3	$\frac{1}{3}\sqrt{g_1^2 + g_2^2 + g_3^2}$	g'_1	g'_2	g'_3	relaxation time (s) at 2K and 0.1 Tesla
1 DMSO	calculation	80	0.203	170	1.918	2.437	2.795	2.410	1.92	3.32	6.90	
	Susceptibility	68(1)	fixed 0	136	-	-	-	2.610(7)	2.61	2.61	5.03	
	HFEPR+FIRMS	71.8	0.17	150	2.10	2.47	2.48					
	HFEPR								1.92	3.59	6.05	
	AC SQUID											$9*10^{-4}$
2 DMF	calculation	111	0.253	242	1.683	2.198	2.989	2.352	2.176	2.805	7.363	
	Susceptibility	90(2)	fixed 0	180	-	-	-	2.687(6)	2.42	2.42	7.02	
	FIRMS			258								
	HFEPR								2.65	2.95	6.55	
	AC SQUID											$2.8*10^{-4}$
3 Py	calculation	85	0.095	172	1.938	2.578	2.713	2.433	2.26	4.22	6.10	
	Susceptibility	75(2)	fixed 0	140	-	-	-	2.531(7)	2.89	2.89	4.80	
	HFEPR+FIRMS	91.3	0.04	183	2.46	2.46	2.60					
	FIRMS											
	HFEPR								2.58	4.60	5.21	
	AC SQUID											$4.7*10^{-4}$
4 PyPhCO	calculation	99	0.053	199	1.926	2.551	2.701	2.416	2.62	4.60	5.57	
	Susceptibility	80(1)	fixed 0	160	-	-	-	2.605(1)	2.92	2.92	6.46	
	FIRMS			193?								
	HFEPR								3.15	3.78	5.58	
	AC SQUID											$2.6*10^{-4}$

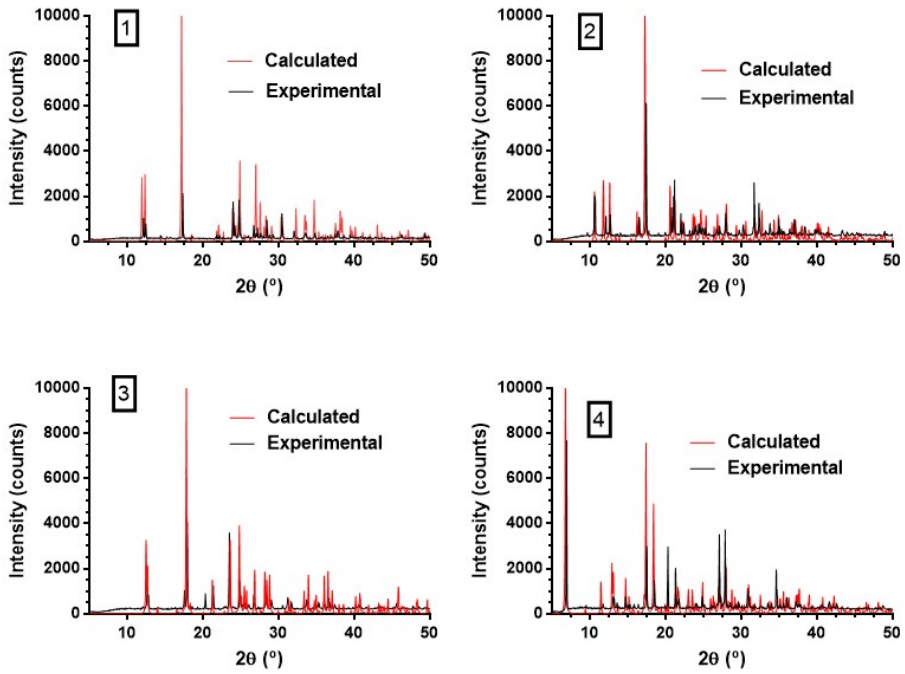

Figure S1. Experimental XRPD for bulk samples of complexes **1**-**4** (red colour) and those derived from their X-Ray crystal structures (black colour)

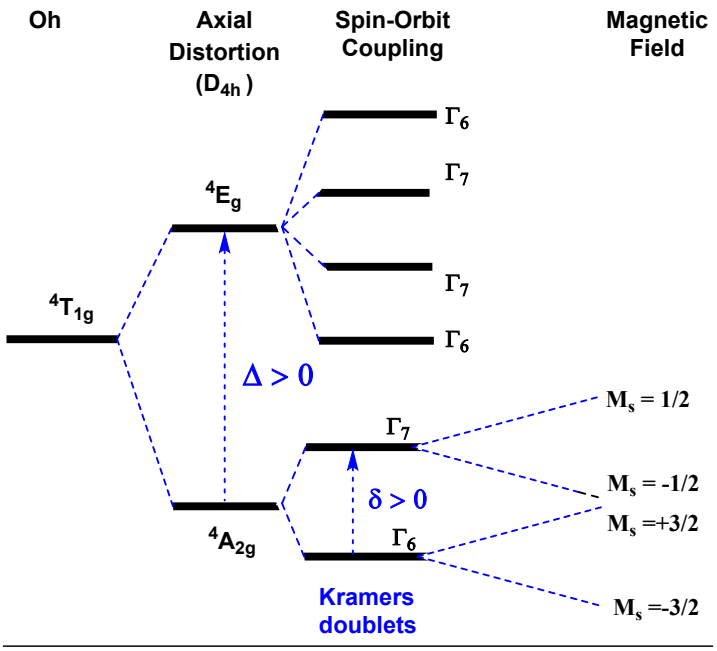

Figure S2.- *Simplifi*ed Energy Level Diagram for the Splitting of the $^4T_{1g}$ Ground State by an axial crystal field , second-order SOC and external magnetic field. D is the axial orbital splitting of the $^4T_{1g}$, while d is the energy gap between the ± 3/2 and ±1/2 Kramers doublet provoked by the second order SOC.

d_{x2-y2} 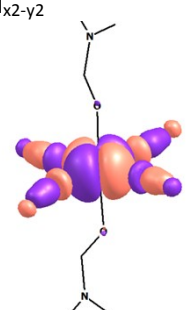	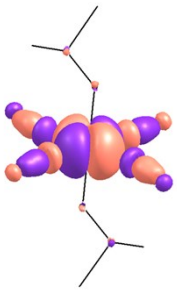 d_{x2-y2}	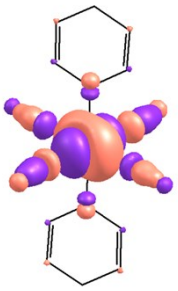 d_{x2-y2}	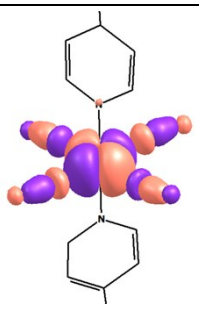 d_{x2-y2}
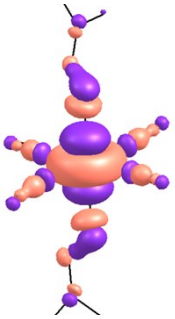 d_{z2}	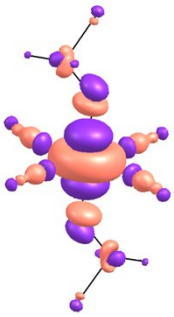 d_{z2}	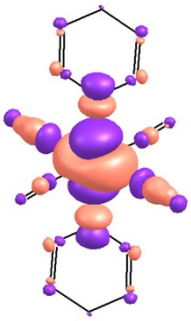 d_{z2}	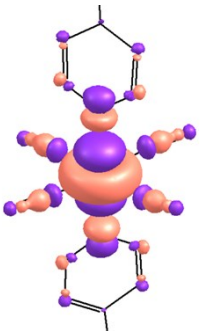 d_{z2}
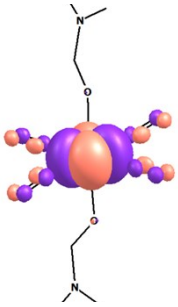 d_{xy}	d_{xy} 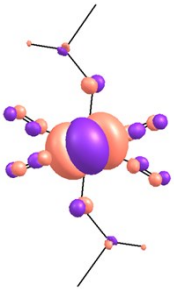	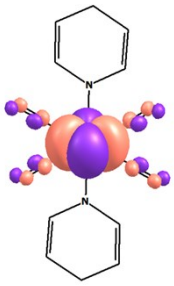 d_{xy}	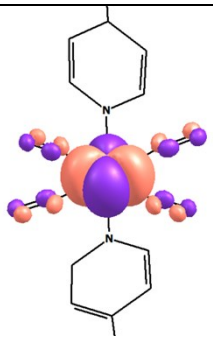 d_{xy}
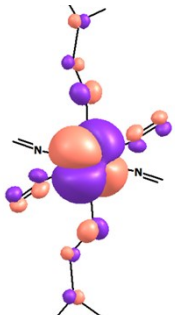 d_{xz}	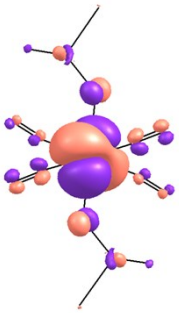 d_{xz}	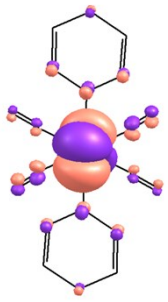 d_{xz}	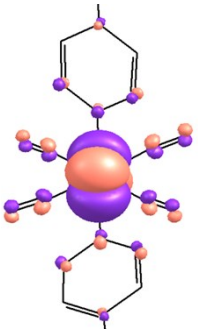 d_{xz}
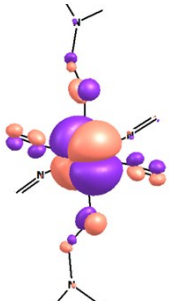 d_{yz}	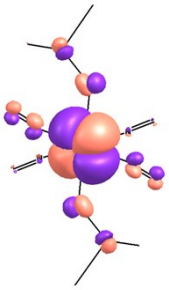 d_{yz}	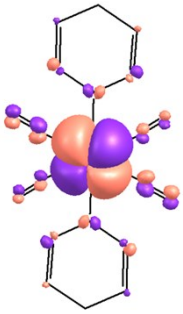 d_{yz}	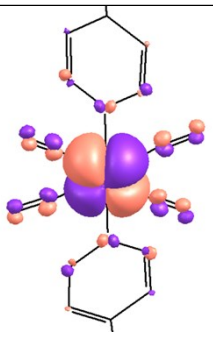 d_{yz}

Figure S3. Ab initio ligand field orbitals excluding gold (I) atoms

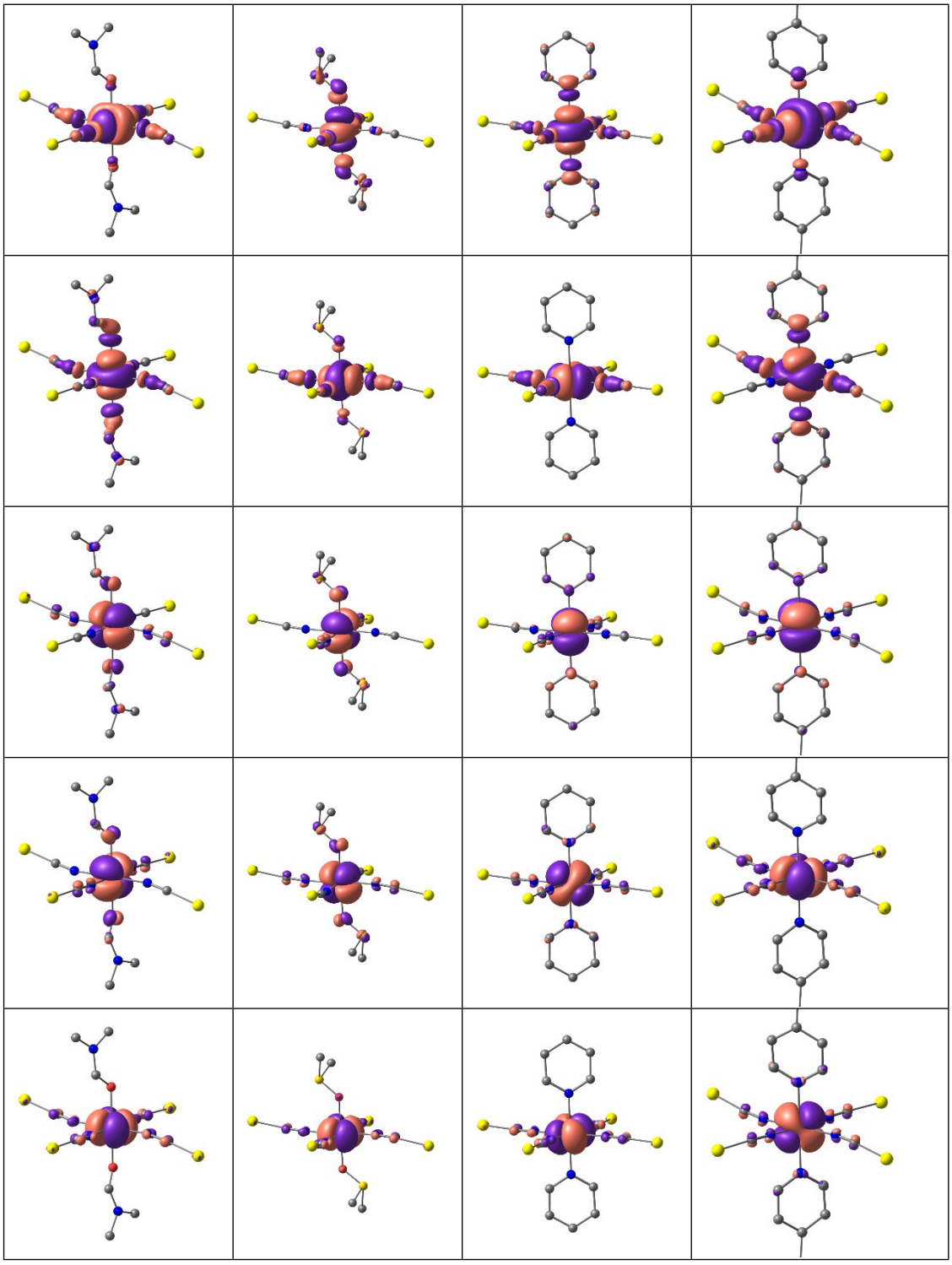

Figure S4. Ab initio ligand field orbitals including gold (I) atoms

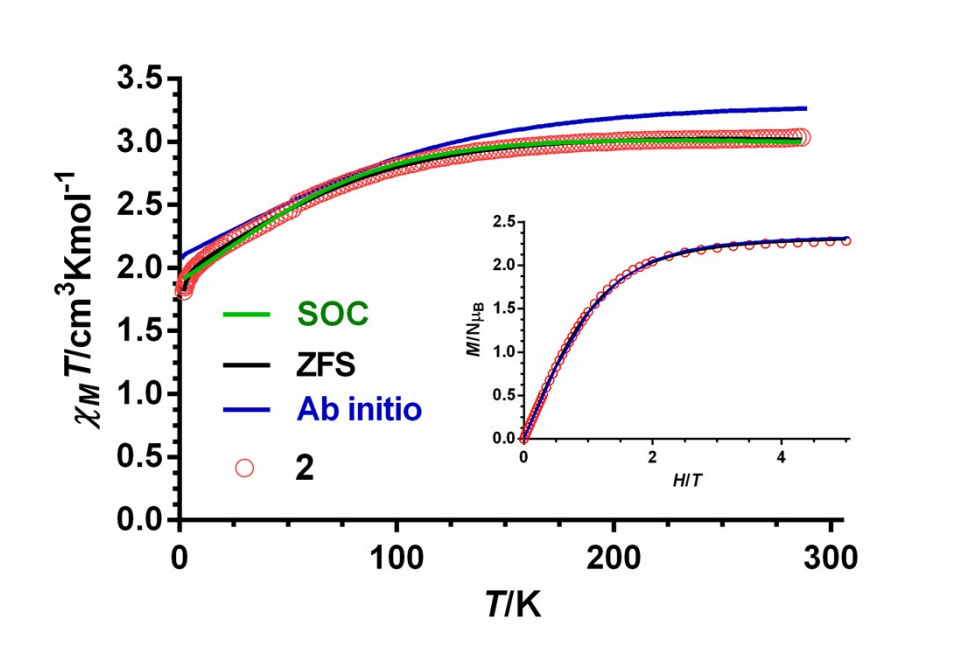

Figure S5 .- Temperature dependence of $\chi_M T$ for compound **2** (red circles). Black and green solid lines represent the best fit to equations 1 and 2, respectively. Blue solid line generated from the *ab* initio calculated energy levels including gold(I) atoms.

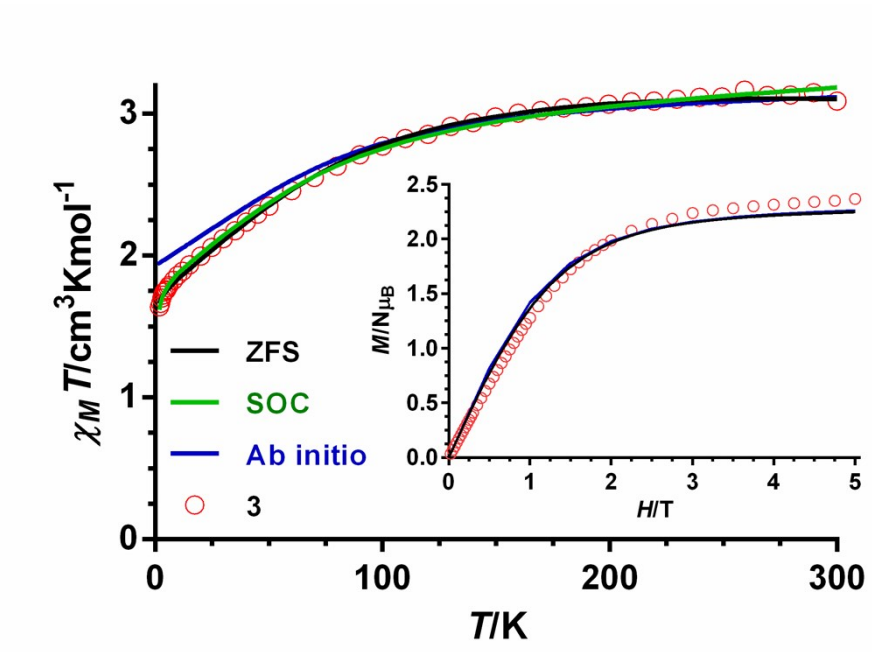

Figure S6 .- Temperature dependence of $\chi_M T$ for compound **3** (red circles). Black and green solid lines represent the best fit to equations 1 and 2, respectively. Blue solid line generated from the *ab* initio calculated energy levels including gold(I) atoms.

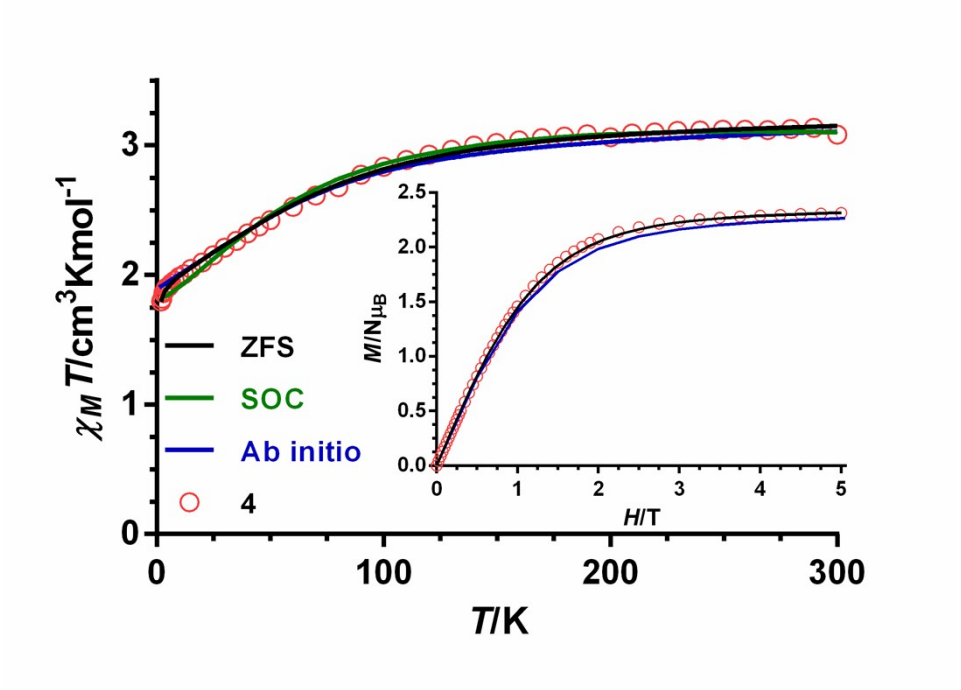

Figure S7.- Temperature dependence of $\chi_M T$ for compound **4** (red circles). Black and green solid lines represent the best fit to equations 1 and 2, respectively. Blue solid line generated from the *ab* initio calculated energy levels including gold(I) atoms.

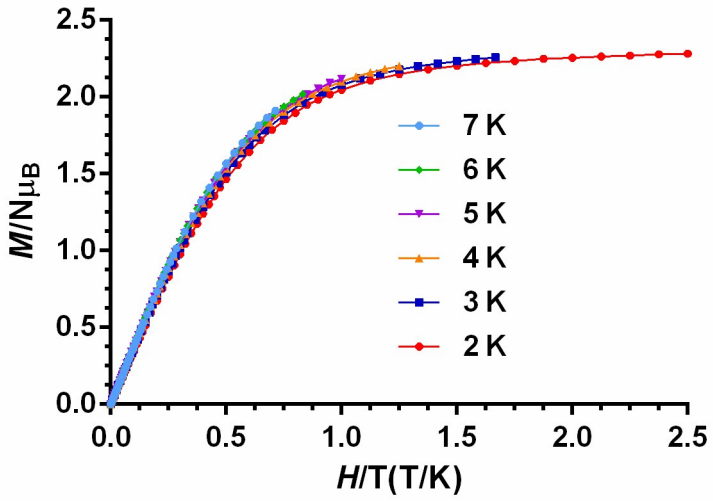

Figure S8.- *M* vs *H/T* isotherms for compound **2** at the indicated temperatures.

.

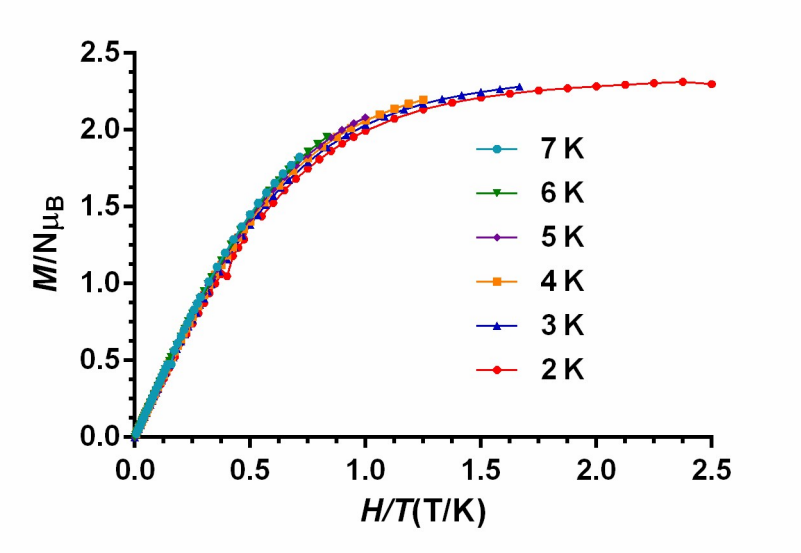

Figure **S9**.- *M* vs *H/T* isotherms for compound **3** at the indicated temperatures.

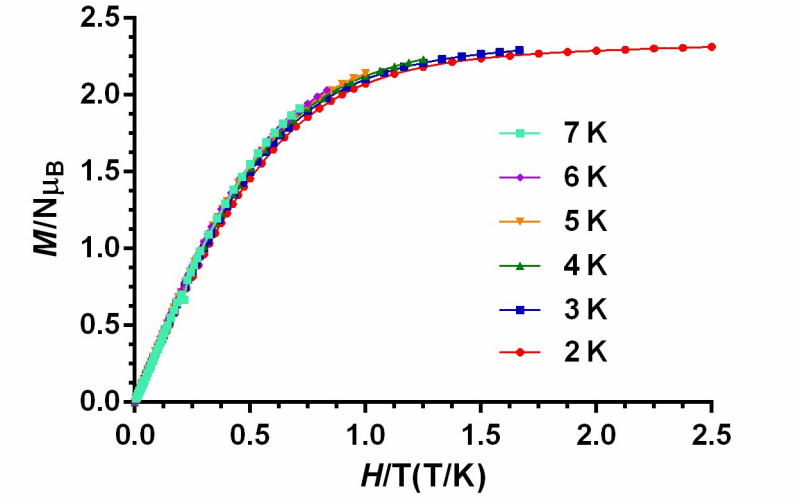

Figure **S10**.- *M* vs *H/T* isotherms for compound **4** at the indicated temperatures.

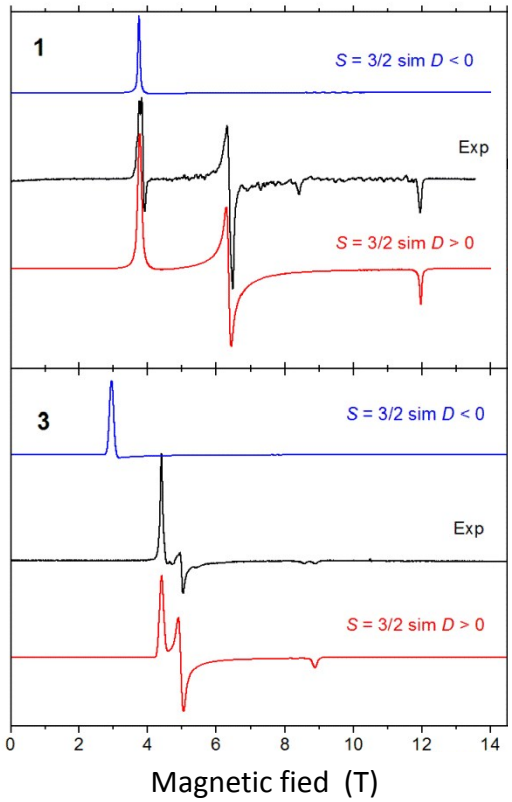

Figure S11. Top: an EPR spectrum of **1** at 321.6 GHz and 7 K accompanied by simulations using $S = 3/2$ spin Hamiltonian parameters: $|D| = 71.8$ cm^{-1}, $|E| = 12.4$ cm^{-1} ($E/D = 0.17$); $g_x = 2.47$; $g_y = 2.48$; $g_z = 2.10$. Bottom: an EPR spectrum of **3** at 321.6 GHz and 10 K accompanied by simulations using $S = 3/2$ spin Hamiltonian parameters: $|D| = 91.3$ cm^{-1}, $|E| = 3.65$ cm^{-1} ($E/D = 0.04$); $g_x = 2.46$; $g_y = 2.46$; $g_z = 2.60$. The g_z value is tentative only since there are two features in the same high-g spectral range and either one could be the parallel turning point. The HFEPR spectra of **2** and **4** cannot be simulated using $S = 3/2$ spin Hamiltonian parameters but only an effective $S = 1/2$ Hamiltonian (Figure S12)

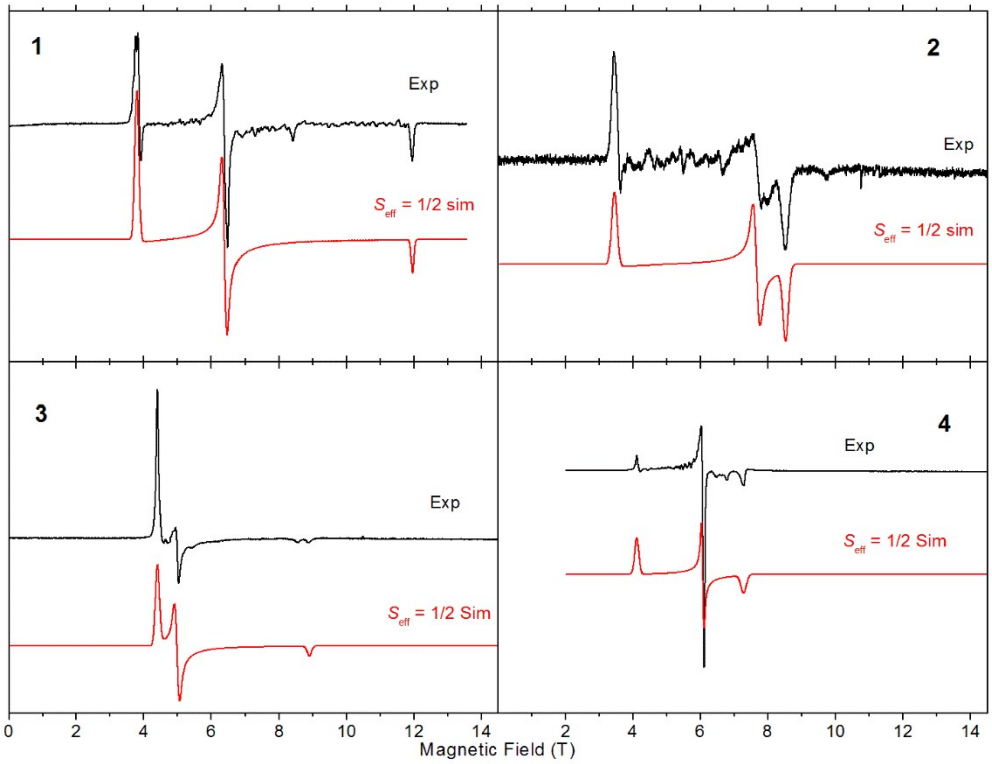

Figure S12.- HFEPR spectra of **1**-**4** at 321.6 GHz (**1**, **3** and **4**), 316.8 GHz (**2**), and 7 K (**1** and **4**) and 10 K (**2** and **3**). Simulations using an effective $S = 1/2$ Hamiltonian appear as red lines. Hamiltonian parameters appear above in Table S4.

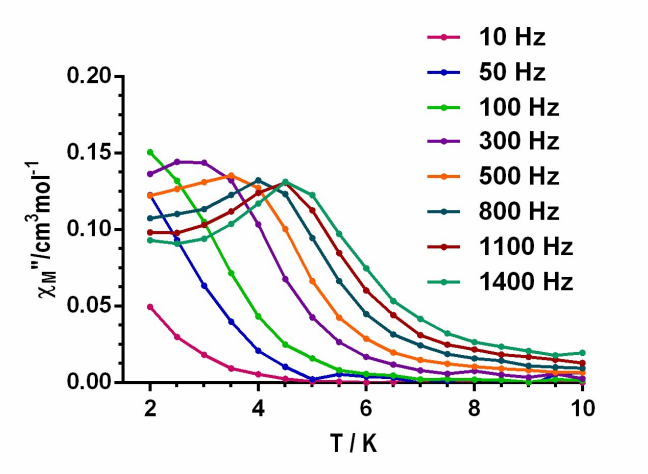

Figure S13.- Temperature dependence of the out-of–phase (χ") for **1** under a H_{dc} = 0.1 T Oe at different frequencies

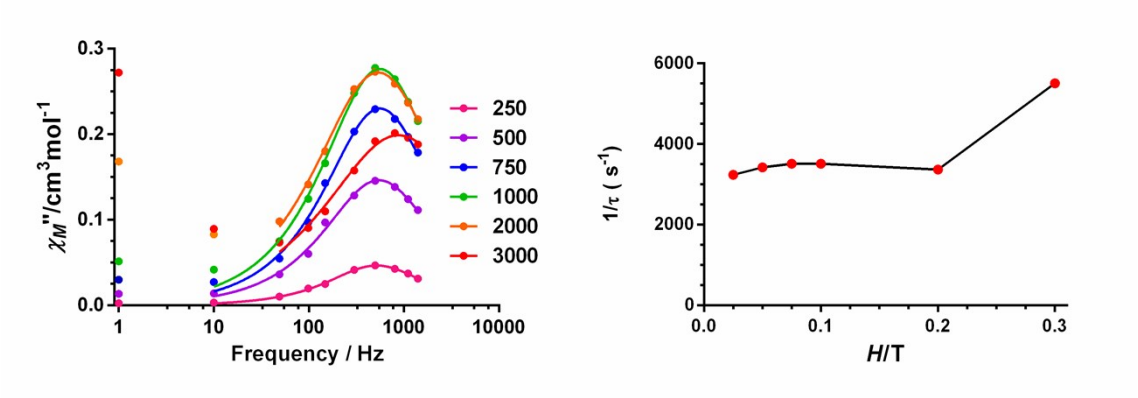

Figure S14.- Field dependence of the out-of-phase signal (χ''_M) at 2 K for **2** (left). Field dependence of the relaxation times for **2** (right).

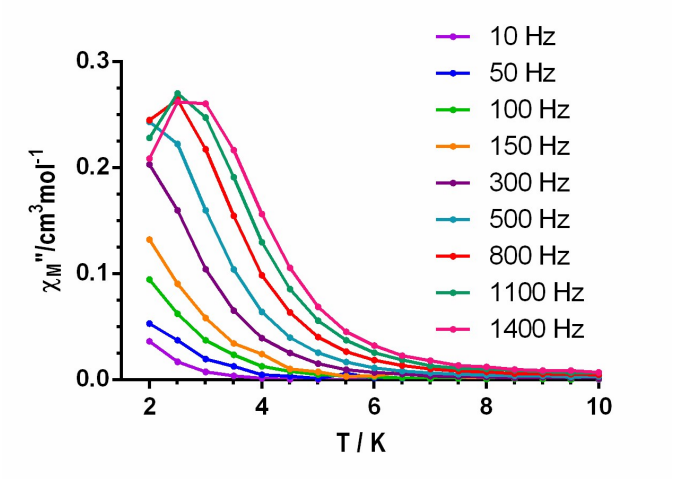

Figure S15.- Temperature dependence of the out-of–phase (χ") for **2** under a H_{dc} = 0.1 T Oe at different frequencies

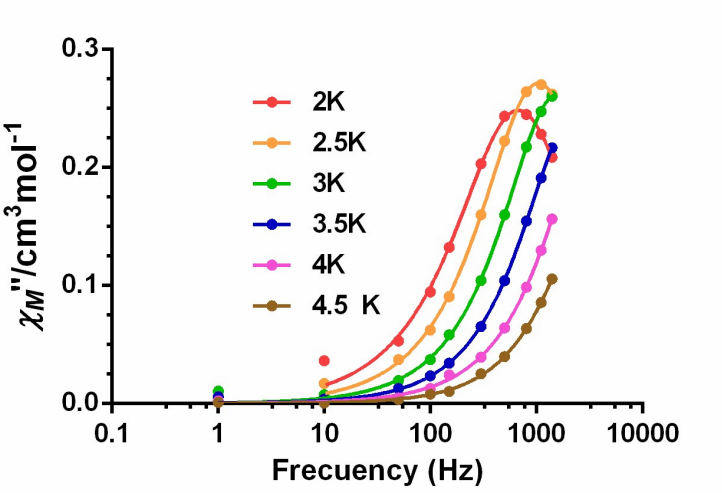

Figure S16.- Frequency dependence of the out-of–phase (χ”) for **2** under a H_{dc} = 0.1 T at different temperatures.

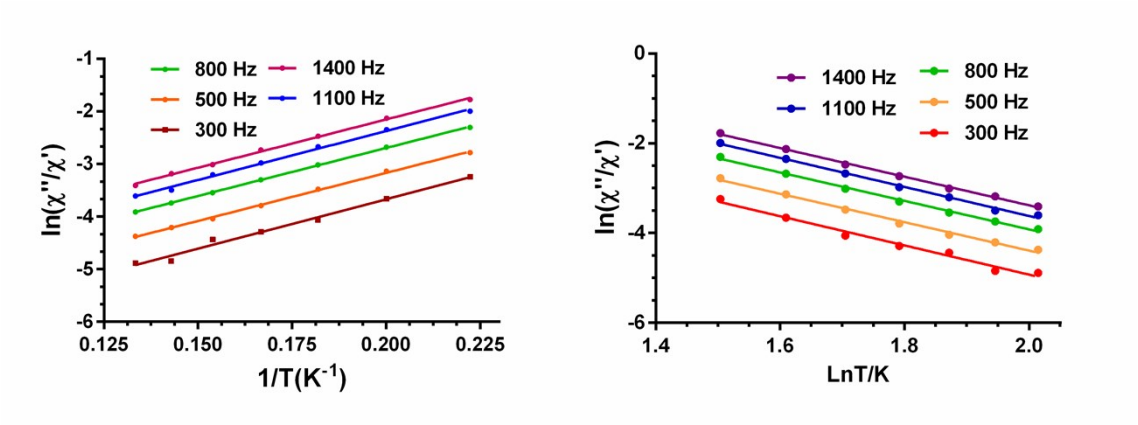

Figure S17.- Temperature dependence of the ratio of the in-phase and out-of-phase ac components at different frequencies under a magnetic field of 0.1 T for **2**. Solid lines correspond to the fit of the experimental data to equation 6 (left) and equation 7 (right).

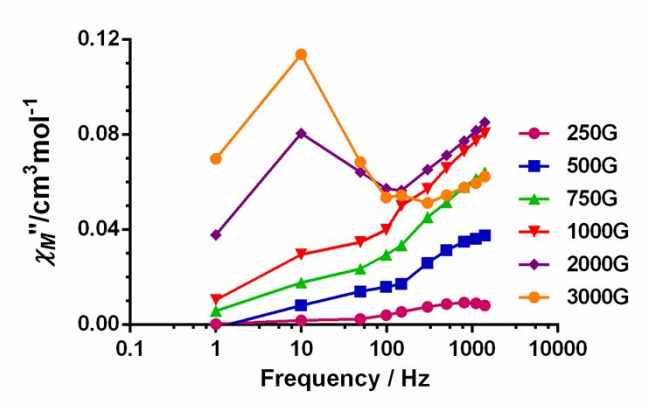

Figure S18.- Field dependence of the out-of-phase signal (χ''_M) at 2 K for **3**

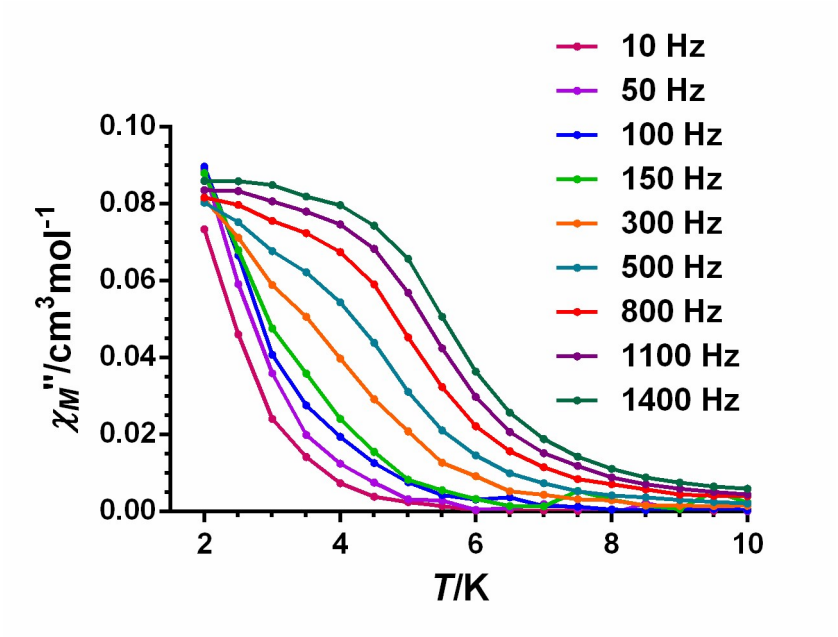

Figure S19.- Temperature dependence of the out-of–phase (χ”) for **3** under a H_{dc} = 0.1 T Oe at different frequencies

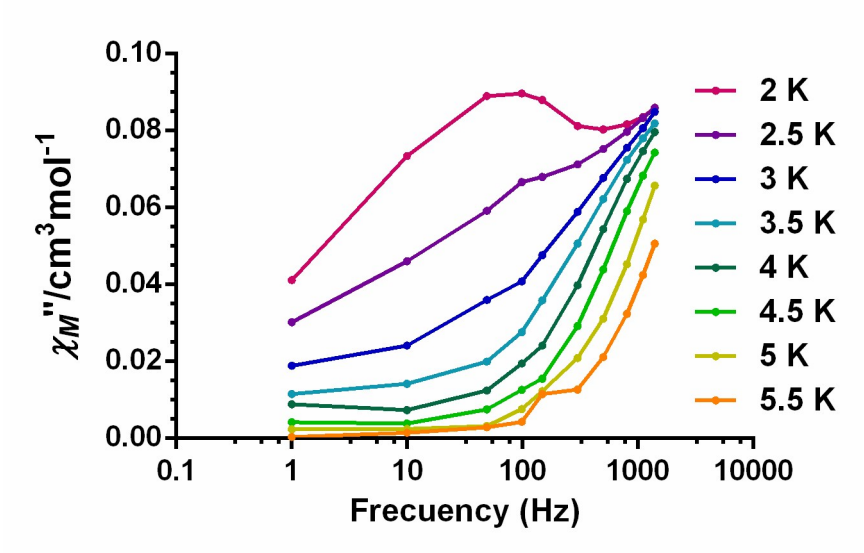

Figure S20.- Frequency dependence of the out-of–phase (χ") for **3** under a H_{dc} = 0.1 T at different temperatures.

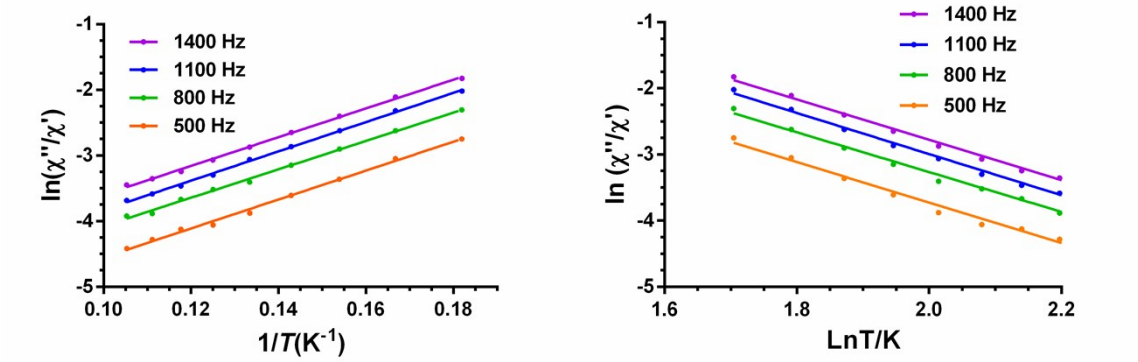

Figure S21.- Temperature dependence of the ratio of the in-phase and out-of-phase ac components at different frequencies under a magnetic field of 0.1 T for **3**. Solid lines correspond to the fit of the experimental data to equation 6 (left) and equation 7 (right).

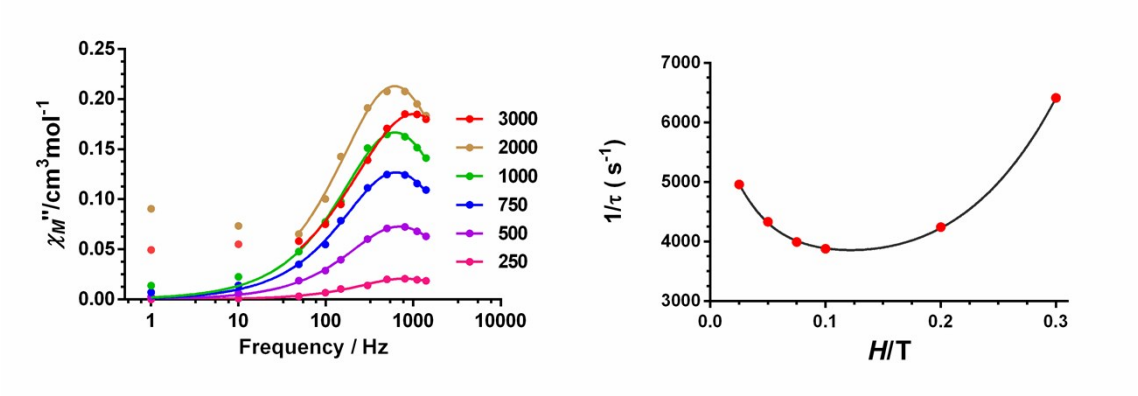

Figure S22.- Field dependence of the out-of-phase signal (χ''_M) at 2 K for **4** (left). Field dependence of the relaxation times for **4** (right).

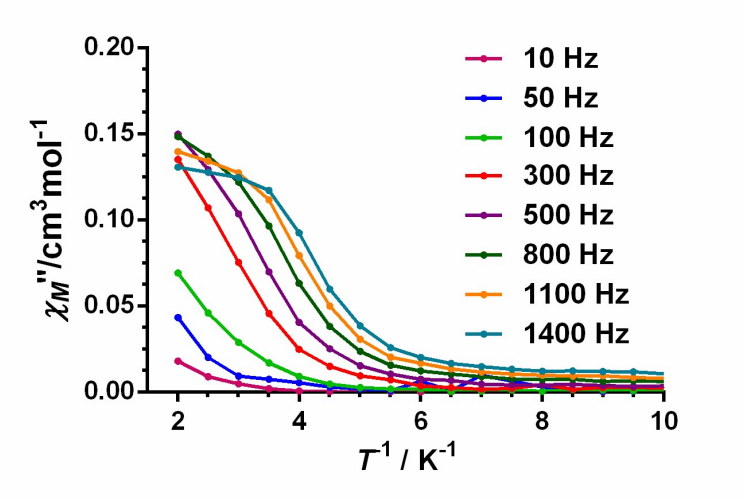

Figure S23.- Temperature dependence of the out-of–phase (χ") for **4** under a H_{dc} = 0.1 T Oe at different frequencies

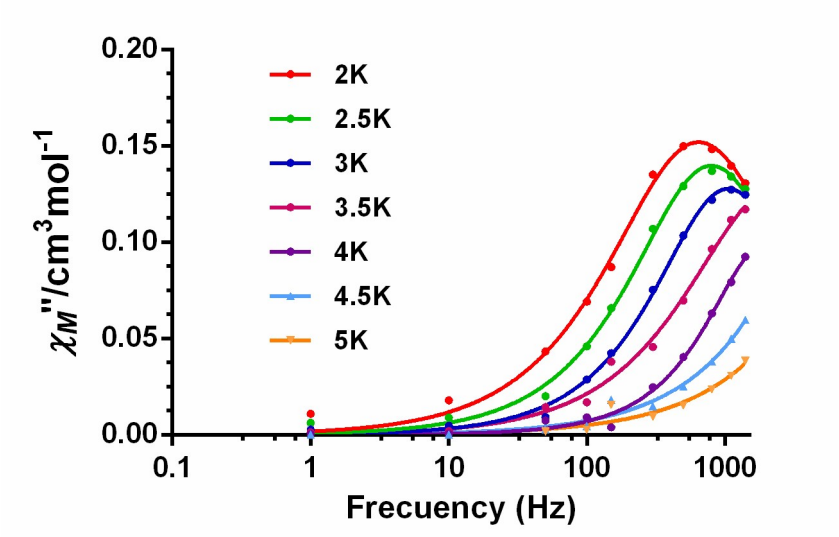

Figure S24.- Frequency dependence of the out-of–phase (χ”) for **4** under a H_{dc} = 0.1 T at different temperatures.

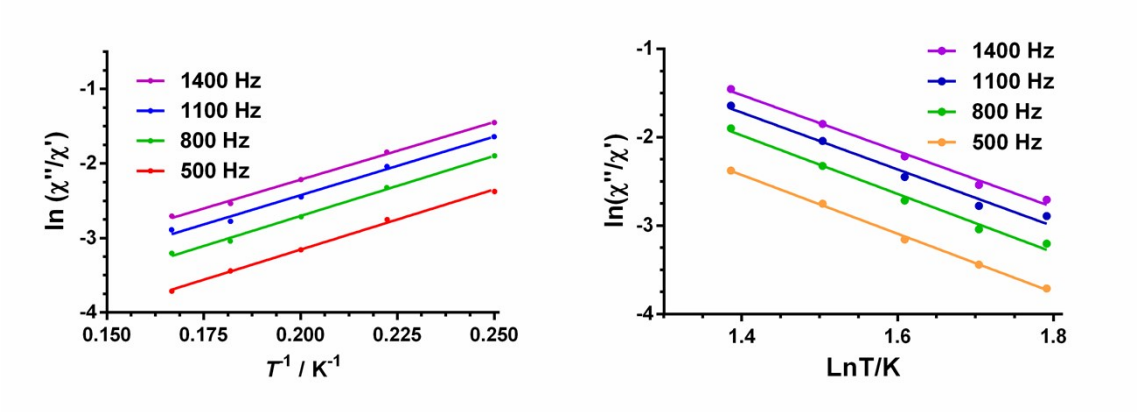

Figure S25.- Temperature dependence of the ratio of the in-phase and out-of-phase ac components at different frequencies under a magnetic field of 0.1 T for **4**. Solid lines correspond to the fit of the experimental data to equation 6 (left) and equation 7 (right).

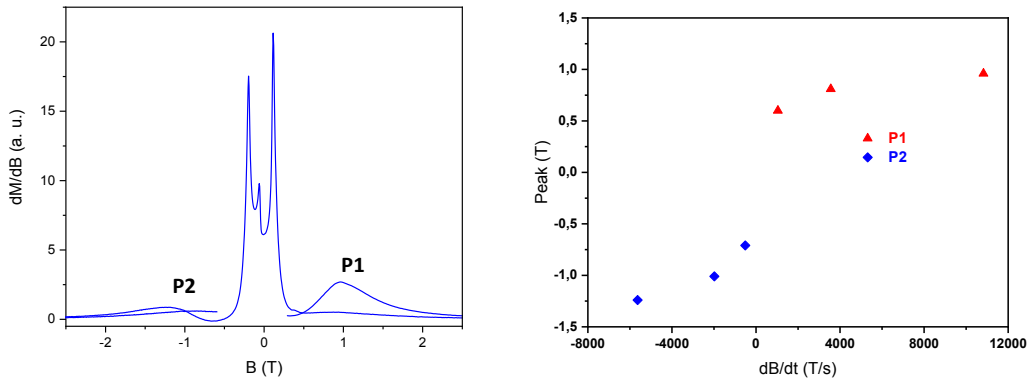

Figure S26.- Differential of magnetization measured at 0.4 K and 5.2 T/ms (left) and sweep rate dependence of peaks P1-P2 (right) for compound **1**.

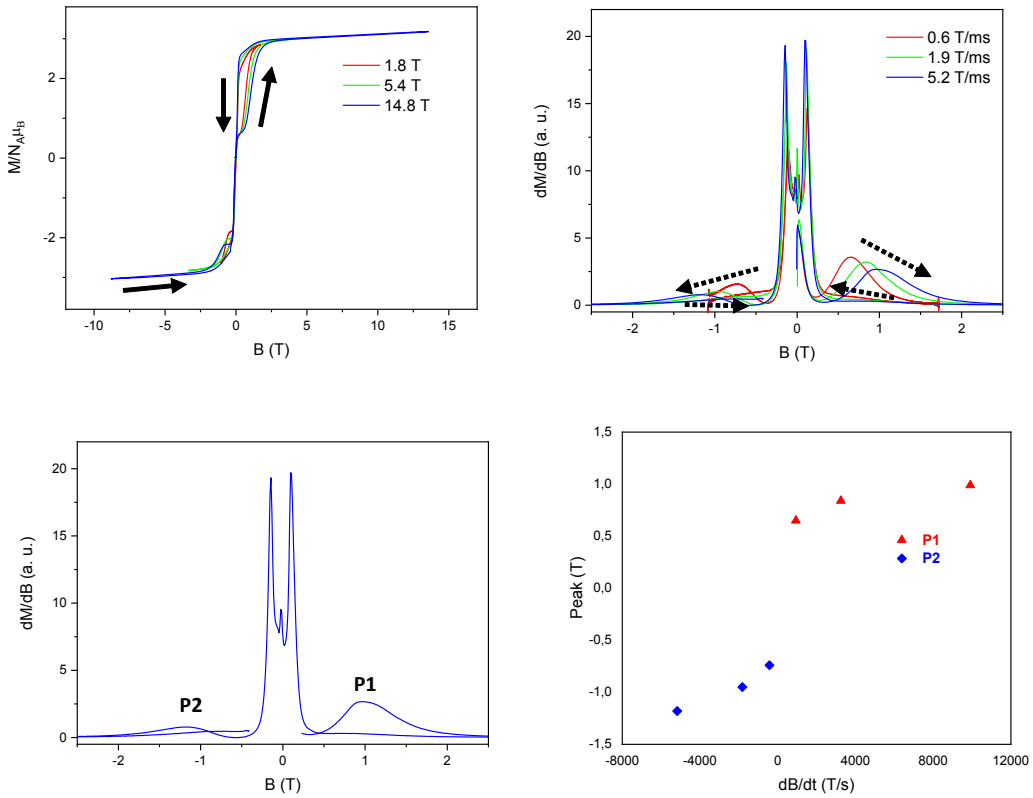

Figure S27.- Pulse-field (top left) and differentiate (top right) magnetizations curves for **2** at 0.4 K and at different scan field rates. Differential of magnetization measured at 0.4 K and 5.2 T/ms (bottom left) and sweep rate dependence of peaks P1-P2 (bottom right) for compound **2**.

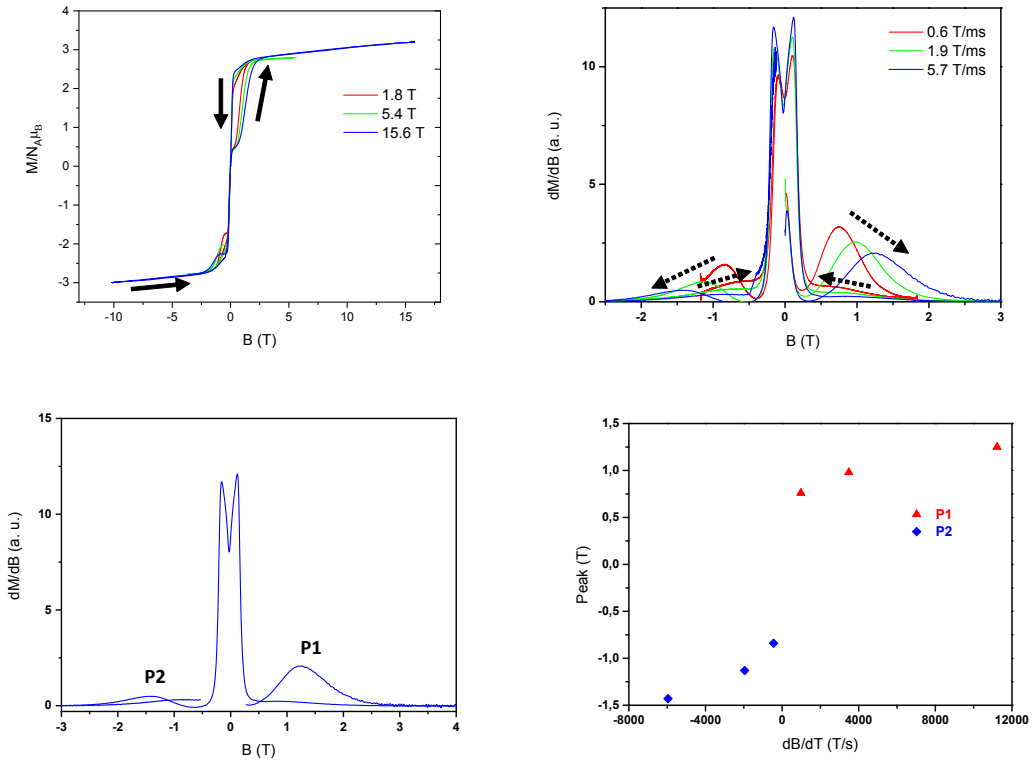

Figure S28.- Pulse-field (top left) and differentiate (top right) magnetizations curves for **3** at 0.4 K and at different scan field rates. Differential of magnetization measured at 0.4 K and 5.2 T/ms (bottom left) and sweep rate dependence of peaks P1-P2 (bottom right) for compound **3**.

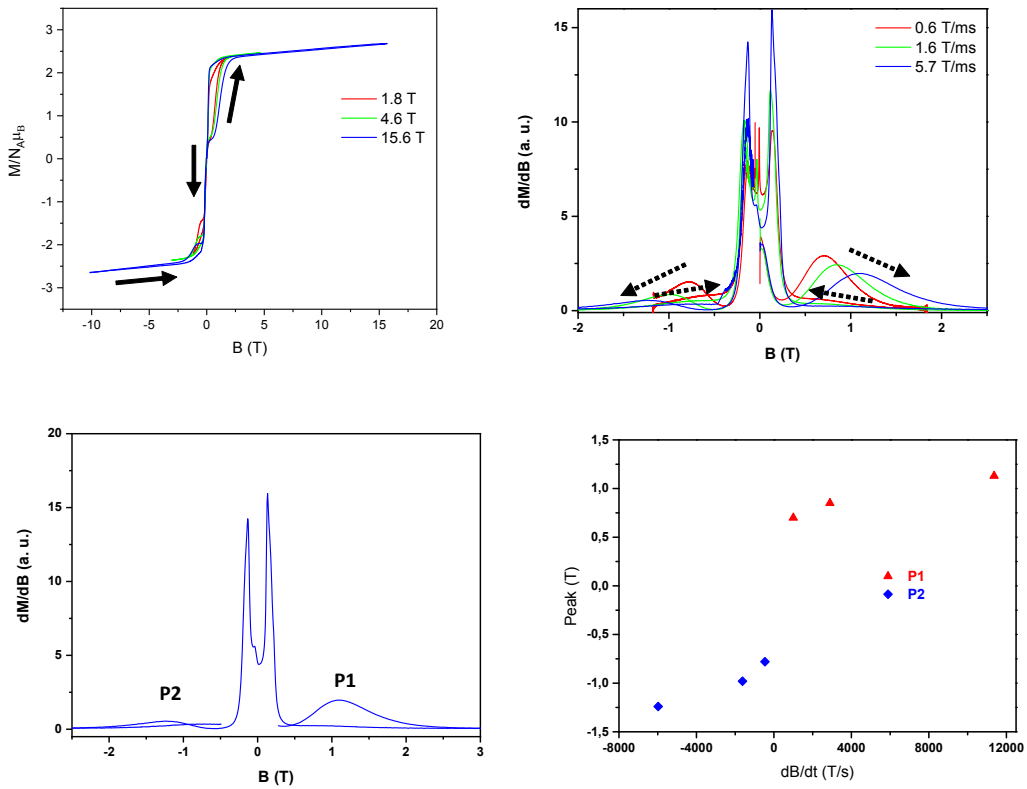

Figure S29.- Pulse-field (top left) and differentiate (top right) magnetizations curves for **4** at 0.4 K and at different scan field rates. Differential of magnetization measured at 0.4 K and 5.2 T/ms (bottom left) and sweep rate dependence of peaks P1-P2 (bottom right) for compound **4**.